# Dynamic Characteristics of Magnetorheological Mounted Metal Rubber Structures Under Multi-physics Coupling Conditions

**Bo PENG [1, 2], Jintao SU [1, 2] *, Jinquan NIE [1]**

[1] *School of Automotive and Traffic Engineering, Hubei University of Arts and Science, Longzhongstreet, 441053, Xiangyang, China*
[2] *Chongqing University of Technology, Shazhong street, 401122, Chongqing, China*

http://doi.org/10.5755/j02.ms.34901

*Received 23 August 2023; accepted 7 November 2023*

To accurately predict the dynamic characteristics of MR mounting, the nonlinear electromagnetic coupling law between MR liquid and soft magnetic material and the solid-liquid interaction, the electromagnetic coupling and fluid-structure coupling mathematical models and numerical simulation models of MR mounting are established. Through the magnetorheological mounting test, the simulation results are compared with the experimental results, and the validity of the numerical simulation model is verified. On this basis, the distribution effect of electromagnetic coupling in a magnetic circuit is analyzed. According to the Bingham model, the variation rule of magnetorheological fluid damping force was deduced. The magnetic field simulation results are introduced into the fluid model and the fluid-solid model, and the fluid-solid coupling effect of the numerical model of magnetorheological mounting is calculated. The dynamic and static characteristics of magnetorheological mounting under different current excitation conditions are simulated. It provides the basis for designing and simulating multi-physical field simulation of MR mounting.
*Keywords:* multiple physical fields, coupling, magnetorheology, mount dynamic characteristics.

## 1. INTRODUCTION

The magnetorheological (MR) mount has the characteristics of fast response speed, high reliability and low energy consumption. Under low frequency conditions, it can provide large stiffness and damping of a wider frequency, which is of great engineering value [1, 2]. Nguyen et al. [3] proposed a magnetorheological mount combined with annular channel and radial channel, and optimized the magnetorheological mount structure by numerical simulation on the Bingham model of magnetorheological fluid. The results show that the damping characteristics of the optimized mount are significantly higher than those of the mount with only an annular channel. Hu Yong [4] designed a shear mode magnetorheological mount, and verified the rationality of the structure through magnetic field analysis. The properties of MR mount and hydraulic mount are compared by experimental test. The experimental results show that the controllability of MR Fluid can better realize broadband vibration isolation. Li [5] designed a magnetorheological mount structure based on the characteristics of squeezed magnetorheological fluid, and proposed a test method for magnetorheological mount. The static and dynamic characteristics of the MR mount were tested and the controllable damping model of the MR mount was established. Constantin Ciocanel et al. [6] designed a magnetorheological mount with a mixture of flow and squeeze modes, analyzed the internal magnetic field distribution of the magnetic circuit structure with different cross-sectional areas and lengths of inertial channels, and tested the dynamic stiffness of magnetorheological mount under different excitation amplitudes. M.O.Bodies [7] designed a ring damped channel magnetorheological mount based on the flow mode magnetorheological fluid. The advantage of the mount is the use of a circumferential channel structure design. By increasing the cross-sectional area of liquid flow, the high frequency dynamic hardening problem of MR mount can be effectively alleviated.

In the structural design and optimization of MR mounting, only the internal magnetic field distribution of MR mounting magnetic circuit is considered, and the output damping force of MR mounting is pushed by the magnetic induction intensity of the damping channel. This method can effectively improve the range of controllable damping force of magnetorheological mounting, but it does not take into account the interaction between rubber and fluid and the influence of multiple physical fields on the performance of magnetorheological mounting. Therefore, it is of great significance to analyze the electric-magnetic and fluid-solid interactions in magnetorheological mounting by using the multi-physics coupling method to predict the properties of magnetorheological mounting.

Tharehalli [8] analyzed the output damping force of MR Dampers under different excitation frequencies by combining ANSYS magnetic field simulation with CFD fluid simulation. The experimental results show that the simulation results agree well with the experimental results. In this study, the coupling mechanism of multi-physical field coupling was studied. Yu [9] established the fluid-solid and magneto-current coupling model of the MR Shock absorber through ADINA software. The magnetic field distribution, stress distribution and damping characteristic

* Corresponding author. Tel.: +86-13618364179.
E-mail: *11947@hbuas.edu.cn* (J. Su)

curves of MR Fluid are obtained by simulation analysis, and the validity of the multi-physics coupling model is verified by experiments. Song [10] carried out magnetic field analysis on the magnetic circuit structure of MR Damper through ANSYS software, obtained the relationship between the current distribution at the damping channel and the magnetic induction intensity distribution, and applied the obtained results to the fluid for finite element analysis, obtained the relationship between the output damping force of the damper and the flow rate.

To accurately predict the structural characteristics of metal and rubber of MR mounting, understand the nonlinear magnetization law between MR Liquid and soft magnetic material and the solid-liquid interaction, the mathematical and numerical simulation models of electromagnetic coupling and fluid-structure coupling of MR mounting were established. Through the magnetorheological test, the validity of the numerical simulation model is verified, and the distribution of electromagnetic field in the magnetic circuit is analyzed. According to the Bingham model, the variation rule of magnetorheological fluid viscosity was deduced. The stress distribution of magnetorheological fluid in the damped channel under different magnetic fields is simulated by introducing the magnetic field simulation results into the fluid model and the fluid-solid model respectively. The dynamic characteristics of magnetorheological mounting with different currents are studied by simulation. It provides the theoretical basis and data foundation for the structural design of MR mounting.

## 2. MAGNETO-RHEOLOGICAL MOUNTING STRUCTURE

Fig. 1 shows the principle diagram of the MR mount structure. The magnetic core assembly has an axisymmetric structure, which divides the mount cavity into upper and lower liquid chambers. The electromagnetic coil is wound on the magnetic core base, and an aluminum alloy partition is used to prevent magnetic leakage. The magnetic conductive material is DT4C material.

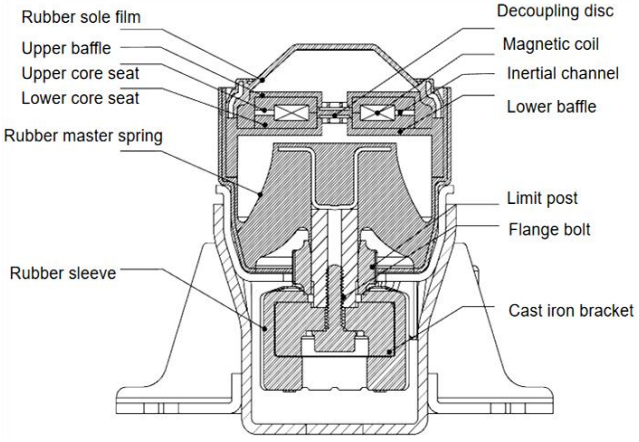


**Fig. 1.** Schematic diagram of MR mount structure

Fig. 2 is a schematic diagram of the MR mount magnetic circuit structure 1/4. When the engine is working, it drives the connecting rod to vibrate. The connecting rod forces the magnetorheological fluid to flow between the upper and lower cavities through vibration. The magnetorheological mount is controlled to produce different output damping forces by varying the current on the coil.

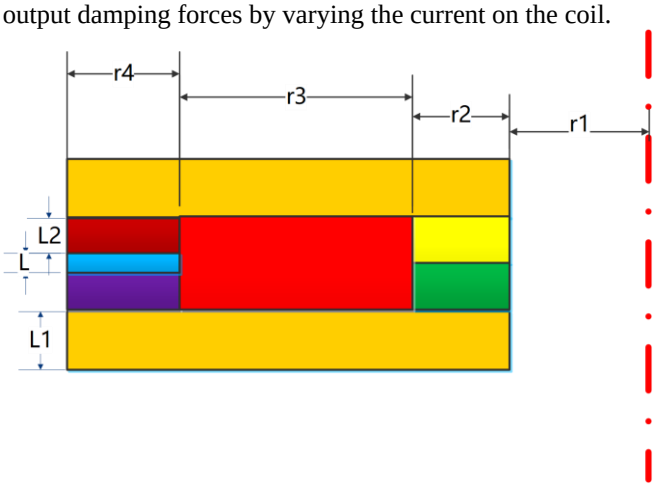


**Fig. 2.** Schematic diagram of magnetic circuit structure 1/4: r1 – inner radius of upper and lower magnetic cores; r2 – coil seat width; r3 – coil width; r4 – width of fluid flow channel; L – height of fluid flow channel; L1 – height of the magnet; L2 – core height

## 3. MULTI-PHYSICAL FIELD COUPLING THEORETICAL MODEL

### 3.1. Magnetic-current coupling model

For a constant magnetic field, the integral form of Maxwell's equations is [11 – 13]:

$$\begin{cases} \oint_s \vec{B} \cdot d\vec{S} = 0 \\ \oint_l \vec{E} \cdot dl = -\iint_s \frac{\partial \vec{B}}{\partial t} \cdot d\vec{S} \\ \oint_l \vec{H} \cdot dl = \vec{I_0} + \iint_s \frac{\partial \vec{D}}{\partial t} \cdot d\vec{S} \\ \oint_s \vec{D} \cdot d\vec{S} = q_0 \end{cases}. \quad (1)$$

For a constant magnetic field, Maxwell's equations of differential equations are:

$$\begin{cases} \nabla \cdot \vec{D} = \rho \\ \nabla \cdot \vec{E} = 0 \\ \nabla \cdot \vec{H} = \vec{J} \\ \nabla \cdot \vec{B} = 0 \end{cases}, \quad (2)$$

where $\vec{D}$ is the flux density (C/m$^2$); $\rho$ is the charge density (C/m$^3$); $\vec{H}$ is the magnetic field strength (A/m); $\vec{J}$ is the current density (A/m$^2$); $\vec{B}$ is the magnetic induction intensity (T). Where, the relationship between $\vec{D}$ and $\vec{E}$, $\vec{B}$ and $\vec{H}$ is [14, 15]:

$$\begin{cases} \vec{D} = \varepsilon_0 \vec{E} \\ \vec{B} = \varepsilon_0 \vec{H} \\ \vec{J} = \sigma \vec{E} \end{cases}, \quad (3)$$

where symbol $\varepsilon_0$ represents capacitance ($F/m$); $\sigma$ represents electrical conductivity ($S/m$).

### 3.2. Fluid-structure coupling model

In the fluid-structure coupling process, the force of the fluid is exerted on the structure, and the deformation of the structure affects the fluid region in turn. The basic kinematic and dynamic conditions at the fluid-structure coupling interface are as follows:

$$d_s = d_f; \tag{4}$$

$$\vec{n} \cdot \tau_s = \vec{n} \cdot \tau_f , \tag{5}$$

where $d_S$ is the structural displacement (m); $d_f$ is the fluid displacement (m); $\vec{n}$ is the normal direction of the coupled boundary; $\tau_s$ is the structural stress (N/mm$^2$); $\tau_f$ is the fluid stress (N/mm$^2$).

According to the dynamic condition (Eq. 5), the fluid concentration force on the structural node on the fluid-structure coupling boundary is:

$$F_s(t) = \int h^d \tau_f \cdot d_s , \tag{6}$$

where $h^d$ is the Nodal displacement (m); $F_S(t)$ is the concentration force on a structural node (N).

The fluid-structure coupling problem is divided into bi-directional coupling and unidirectional coupling. Among them, when the fluid force affects the deformation of the structure and the structural displacement affects the shape of the flow field, the correlation analysis of this kind of problem is called "two-way coupling". When the effect of structural deformation on the fluid is ignored, this type of coupling is called "one-way coupling". The solid part of the material of the magnetorheological mounting interacting with the fluid is rubber, and the rubber material is easily deformed when subjected to external forces. Therefore, the fluid-structure coupling of MR mounting should be bidirectional.

For two-way coupling problems, ADINA provides a simple direct coupling method (also known as the synchronous solution method), the solution equation is as follows [12, 13]:

$$\begin{bmatrix} A_{ff} & A_{fs} \\ A_{sf} & A_{ss} \end{bmatrix} \begin{bmatrix} \Delta X_f^k \\ \Delta X_s^k \end{bmatrix} = \begin{bmatrix} B_f \\ B_S \end{bmatrix}; \tag{7}$$

$$X^{k+1} = X^k + \Delta X^k , \tag{8}$$

where $X_f^k$ is the pressure and velocity vectors of the kth fluid unit; $X_s^k$ is the pressure and displacement vectors of the kth structural element.

The direct coupling method has the advantages of fast operation speed and easy convergence. In this paper, the multi-physics coupling simulation of the magnetorheological suspension model is solved by the direct coupling method.

## 4. MAGNETORHEOLOGICAL MOUNTING TEST

To test the working performance of the optimized magnetorheological mount, this chapter processed the designed magnetorheological mount test sample, and built a test system for its dynamic performance experimental analysis. The feasibility of the structure design, the accuracy of the multi-field coupling simulation and the effectiveness of the multi-objective optimization are further verified according to the experimental results and the comparative analysis between them.

### 4.1. Test sample and equipment

The designed magnetorheological mount sample is fabricated on the basis of hydraulic mount shell, and its main components are aluminum 6061 material and electric pure iron DT4C. CNC machine tool was used to cut and mill the magnetic separator and magnetic loop. The processed magnetic core components and MR mount samples are shown in Fig. 3.

a

b

**Fig. 3.** Magnetorheological core structure and assembly: a – MR core assembly; b – magnetorheological mounting assembly

The magnetorheological mount performance test was carried out in the laboratory. The test equipment mainly includes the Taiwan Yoken *UD3600/400* fatigue testing machine, constant current source, force sensor, displacement sensor, data acquisition instrument, and test computer. The test system is shown in Fig. 4.

### 4.2. Test and result analysis

#### 4.2.1. Analysis of zero field static stiffness results

In mounting testing, the static deformation of the mounting should be considered first, which is the static deformation of the mounting under a certain static load.


**Fig. 4.** Fatigue test machine for magnetorheological mounting

Since the static deformation of the mounting will cause the powertrain to produce a certain displacement in a certain direction, and this static deformation must be controlled within a certain range when the powertrain mounting is matched to prevent the engine powertrain from interfering with other parts of the body, At this time, the static load value is generally set to -3000 N and 1000 N according to engineering experience and the force load of the powertrain mounting point. The working static load range of the MR mount is -3000 – 1000 N. The excitation force and deformation displacement of the MR mount were read, and the static stiffness curve of the MR mount with zero field was drawn, as shown in Fig. 5.

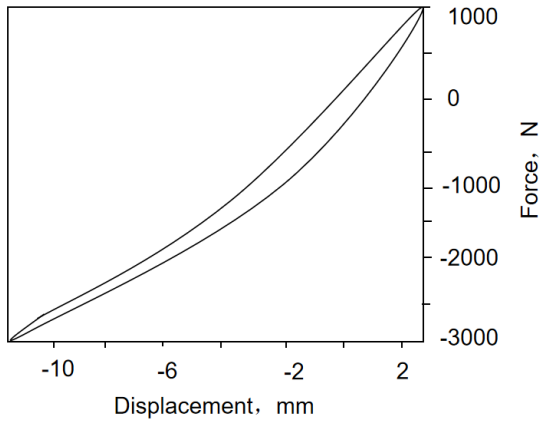


**Fig. 5.** Static stiffness curve of magnetorheological mount

The linear segment in Fig. 5 is selected to calculate the static stiffness of the MR mount, and the result is 215 N/mm, which meets the static stiffness design requirements of engine isolation components.

### 4.2.2. Dynamic characteristics test

The dynamic stiffness of the mount was measured by the hysteresis curve method. Firstly, a 1000 N load was applied to the magnetorheological mount, the amplitude of excitation force was 0.5 mm, and the test frequency was 0 – 50 Hz. Since the actual output damping of the magnetorheological mount is affected by the magnetic field, it is necessary to input different excitation currents to test the dynamic stiffness of the magnetorheological mount. The maximum excitation current of the designed magnetorheological mount is 1.2 A, the test range is 0 – 1.2 A, and the test interval is 0.2 A. The dynamic stiffness curve of MR mount can be measured by reading the exciting force and deformation displacement of MR mount under different current, as shown in Fig. 6.

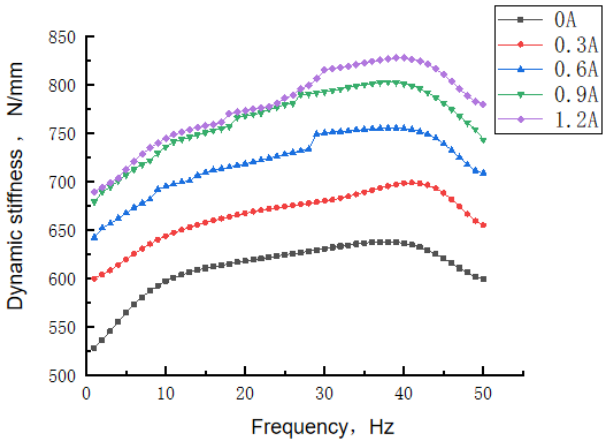


**Fig. 6.** Dynamic stiffness curve of magnetorheological mount

It can be seen from the dynamic stiffness test data that the dynamic stiffness of the magnetorheological mount generally tends to rise regardless of whether current is applied to the mount. When no current is applied, an MR mount is equivalent to a passive hydraulic mount. As can be seen from Fig. 6, the zero-field dynamic stiffness of the mount increases from 0 to 39 Hz. At 38 Hz, the mount dynamic stiffness reaches the maximum value of 636 N/mm, and after 39 Hz, the dynamic stiffness decreases. After the current is applied, it can be seen from the dynamic stiffness variation trend of different current sizes loaded that the dynamic stiffness value increases with the increase of the input current. With the increase of the current, the controlled damping force of the mount increases gradually. On the other hand, when the input current increases from 0.9 A to 1.2 A, the stiffness does not change significantly, because the magnetic saturation operating point has been reached at 1.2 A. When the maximum input current is 1.2 A, the maximum dynamic stiffness is 827 N/mm. This further indicates that the MR mount sample has good controllability in a certain range. Compared with the simulation analysis results, it can be seen that the dynamic stiffness variation rules of the test and simulation are the same.

According to the test analysis of the magnetorheological mount sample, the mount sample has good static and dynamic characteristics. The static stiffness value of the magnetorheological mount sample has good linearity, and the calculated static stiffness value meets the design requirements. The dynamic test results show that the MR mount sample has good controllability. The specific performance is under static test, the static stiffness of the mount is 215 N/mm, which meets the needs of the mount support function. Under the dynamic characteristic test, the dynamic stiffness of MR Also increases gradually with the increasing of applied current, and the maximum adjustable value of dynamic stiffness is 191 N/mm.

#### 4.2.3. Verification of test and simulation results

Since this paper mainly focuses on the maximum dynamic stiffness and adjustable range of MR mount, the

test values and simulation values of MR mount in full field were compared (as shown in Fig. 7). It can be seen from the figure that the test peak frequency of the dynamic stiffness of the MR mount is about 39Hz, and the peak dynamic stiffness is 827 N/mm. The peak frequency of the simulation value is partially earlier than that of the test value, but the overall trend is consistent, and the peak value of the simulation dynamic stiffness is 797 N/mm. The calculated error of dynamic stiffness and test is 3.7 %, which is within the reasonable error range of simulation and test [14, 15].

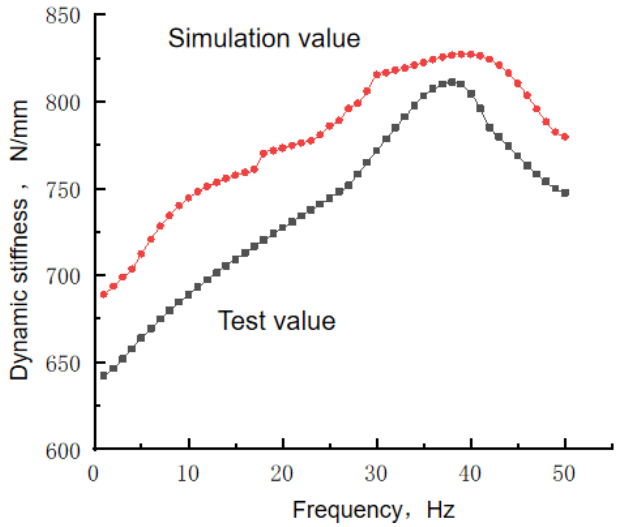


**Fig. 7.** Comparison of test and simulation values

## 5. MULTI-PHYSICAL COUPLING SIMULATION OF MAGNETORHEOLOGICAL MONUNT

The rheological properties of magnetorheological fluid change with the action of a magnetic field, which affects the working performance of magnetorheological mount, including structural parameters, magnetic field parameters and other factors. Therefore, in this chapter, the electric-magnetic and fluid-solid coupling mathematical models of the magnetorheological mount were established, and the finite element simulation models were established respectively in Maxwell and ADINA software. It provides the basis for the structure design and multi-physical field coupling simulation of the MR mount.

### 5.1. Electromagnetic coupling simulation

The magnetorheological fluid material used in this paper was provided by China Institute of Materials Research. Table 1 describes the specific parameters.

Fig. 8 and Fig. 9 show the material data of MR fluid. Because of the nonlinear *B-H* curves of DT4C material and MR fluid, it is impossible to simply use the permeability to analyze the magnetic field. In ORIGIN software, a third-order polynomial is used to fit the material data of MR fluid. The formula is as follows:

$$\tau_B = 1.09 - 58.37B + 878.68B^2 - 987.21B^3; \quad (9)$$

$$\eta = \eta_0 + 0.02 - 1.14B + 17.2B^2 - 19.4B^3. \quad (10)$$

When the excitation current $I$ = 1.2 A, the magnetic induction intensity distribution of magnetic circuit and damping channel is shown in Fig. 10 and Fig. 11.

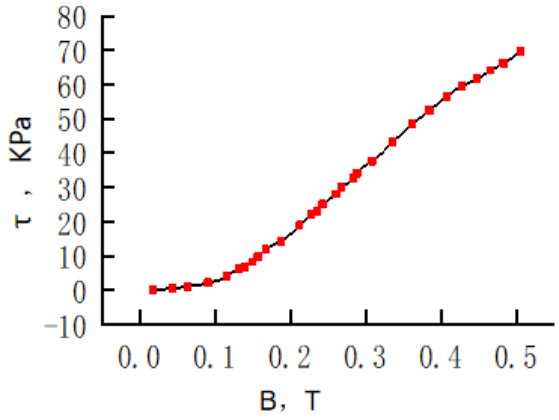


**Fig. 8.** Curve of shear stress-magnetic induction intensity

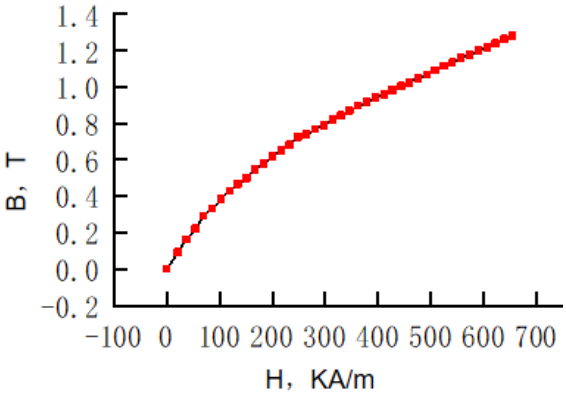


**Fig. 9.** B-H curve

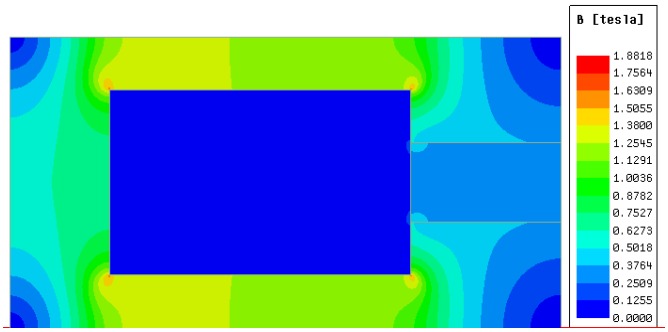


**Fig. 10.** Distribution of magnetic induction intensity

As can be seen from Fig. 11, the maximum magnetic induction is at the corner of the coil slot of the magnetic core, and its maximum magnetic induction is 2.4 T. The simulation results verify the conclusion of [15] that the magnetic flux density distribution is not uniform, which provides a basis for the design optimization of the magnetic circuit of MR mount.

**Table 1.** Material parameters of MRFF-J25T

| Type | Density, g/cm | Operating temperature, ℃ | Zero field viscosity at room temperature Pa·s($\gamma$ = 51/s) | Shear stress, kPa($B$ = 0.5 $T$) |
|---|---|---|---|---|
| MRFF-J25T | 2.65 | -40 ~ 130 | ≤ 1.0 | ≥ 40 |

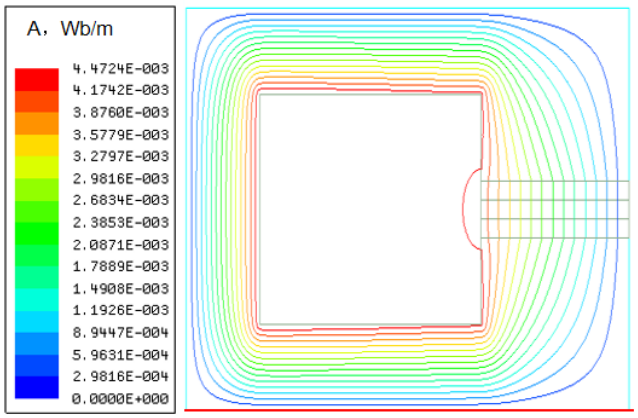


**Fig. 11.** Magnetic field lines

The average magnetic induction intensity is concentrated between 0.8 – 1.1 T. When the maximum working current $I$ = 1.2 A, the magnetic induction intensity distribution at the corresponding channel of the magnetic pole is relatively uniform, and the average magnetic induction intensity is 0.36 T. After repeated simulation of the magnetic circuit structure in the interval (0 – 1.2) A, the average magnetic induction intensity at the damping channel under different current currents can be obtained, as shown in Table 2.

**Table 2.** Relation between current, magnetic induction intensity and shear stress at damping channel

| | | | | | |
|---|---|---|---|---|---|
| $I$, A | 0 | 0.3 | 0.6 | 0.9 | 1.2 |
| $B$, T | 0 | 0.1 | 0.2 | 0.3 | 0.36 |
| $\tau$, kPa | 0 | 3.05 | 14.95 | 33.71 | 47.89 |
| $\eta$, Pa·s | 0 | 0.86 | 1.09 | 1.46 | 1.74 |

Fig.12 shows the viscosity and current curve of MR fluid. As can be seen from the figure, the magnetic induction intensity at the damping channel increases with the increase of the current, making the viscosity of the magnetorheological fluid increase with the increase of the magnetic induction intensity. When the current is 1.2 A, the maximum magnetic inductance is 0.37 T. The response mechanism of magnetic inductance intensity and magnetorheological liquid viscosity to current has verified the theory proposed in reference [13, 15]. The numerical simulation results provide a theoretical basis for the design of MR liquids. When the viscosity of magnetorheological fluid changes, the viscous damping force and coulomb damping force will also change, thus affecting the output performance of the magnetorheological mount.

## 5.2. Magnetorheological fluid damping force calculation

When the gap of the plate remains constant along the direction of fluid movement, the pressure decreases uniformly along the direction of fluid movement. The flow coordinate system between plates is shown in Fig. 13. For incompressible fluid, the Nass-Stokes equation can be simplified as [13]:

$$\frac{\Delta p}{I} = \eta \frac{d^2 \upsilon_y}{dz^2}. \tag{11}$$

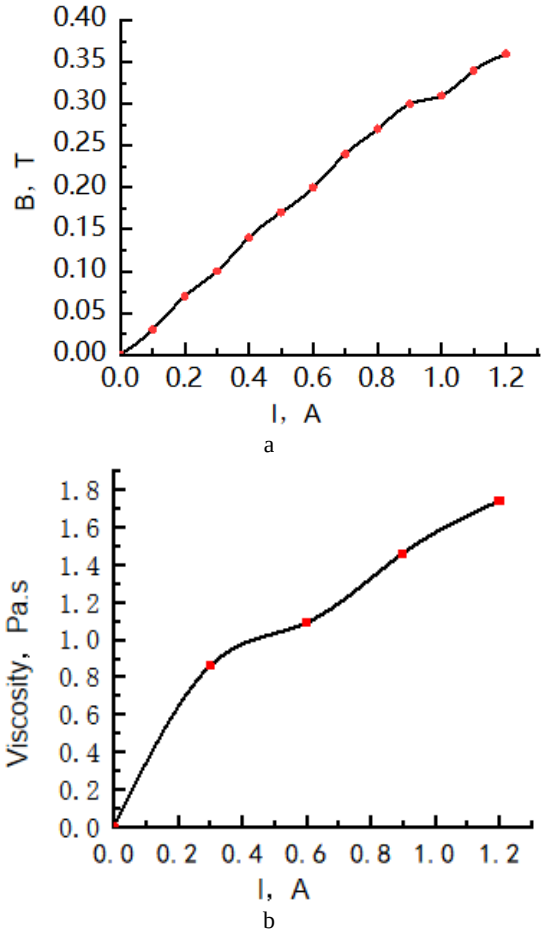


**Fig. 12.** Relation curve between current and viscosity: a – current and magnetic flux relation curve; b – relationship between current and viscosity

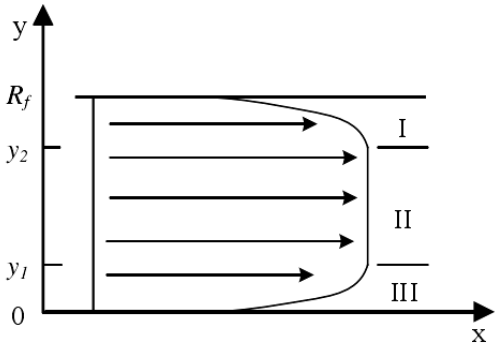


**Fig. 13.** Frame of laminar flow on a plate

The Bingham constitutive relation of magnetorheological fluid can be expressed by the following equation:

$$\tau = \tau_{BZ} sgn\left(dv_y / dz\right) + \eta_0 \left(dv_y / dz\right), \tag{12}$$

where $\tau_{BZ}$ is the yield stress of MR fluid; $d\vartheta_y / dz$ represents the shear rate of the liquid; $\eta_0$ is the viscosity of the magnetorheological fluid at zero magnetic field.

It can be deduced from the above equation that the pressure difference between the two sides of the plate is:

$$\Delta P_m = \frac{12\eta_0 l}{Rh^3} Q_m + \frac{3l}{h} \tau_{BZ}, \tag{13}$$

where $R$ is the length of the cross section, $h$ is the cross-section width, $l$ is the channel length. The damping force of the channel corresponding to the effective pole:

$$F_c = F_\eta + F_\tau = \left( \frac{12\eta_0 l}{Rh^3} Q_m + \frac{3l}{h} \tau_{BZ} \right) A_p, \tag{14}$$

where $A_p$ is the equivalent cross-sectional area of the rubber main spring.

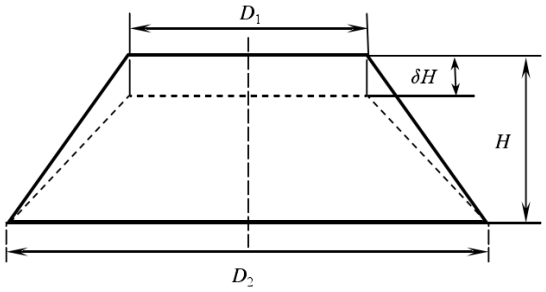


**Fig. 14.** Schematic diagram of deformation of rubber main spring

Fig. 14 shows the force diagram of the rubber main spring. The rubber main spring is not a regular shape, so its equivalent area is difficult to measure directly. It can be estimated by structural parameters:

$$A_p = \frac{\pi}{12}(D_1^2 + D_2^2 + D_1 D_2), \tag{15}$$

where $D_1$ and $D_2$ represent the structural size of the contact surface between the rubber master spring and the magnetorheological fluid. According to the structural parameters of the rubber main spring, it can be obtained: $D_1 = 2r_1 = 50$ mm, $D_2 = 2r_2 = 78.6$ mm. The equivalent piston area of the main rubber spring can be obtained $A_p = 3.299 \times 10^3$ mm$^2$.

## 5.3. Fluid-solid coupling simulation

### 5.3.1. Solid simulation analysis

In HyperMesh software, the magnetorheological mount 3D model is simplified and divided by tetrahedral mesh. After partitioning, the model is imported into ADINA software for processing. The full displacement constraint is added to the metal contact boundary in the solid model to restrict its movement. The boundary that contacts with the fluid part is set as the fluid-structure coupling boundary surface. During the movement of the rubber spring, the magnetorheological fluid is squeezed through the annular damping channel and exerts a force on the damping channel. In the multi-physical field coupling simulation of MR mount, 1000 N preload is applied to the main spring, the frequency is 10 Hz, the amplitude is 0.5mm, and the cloud image of the maximum and minimum displacement of MR mount is shown in Fig. 15. Fig. 15 is a simulation displacement diagram of a magnetorheological mount solid.

According to the simulation results, under 1000 preload, the minimum deformation of the MR mount is 0.1 mm and the maximum deformation is 0.3 mm.

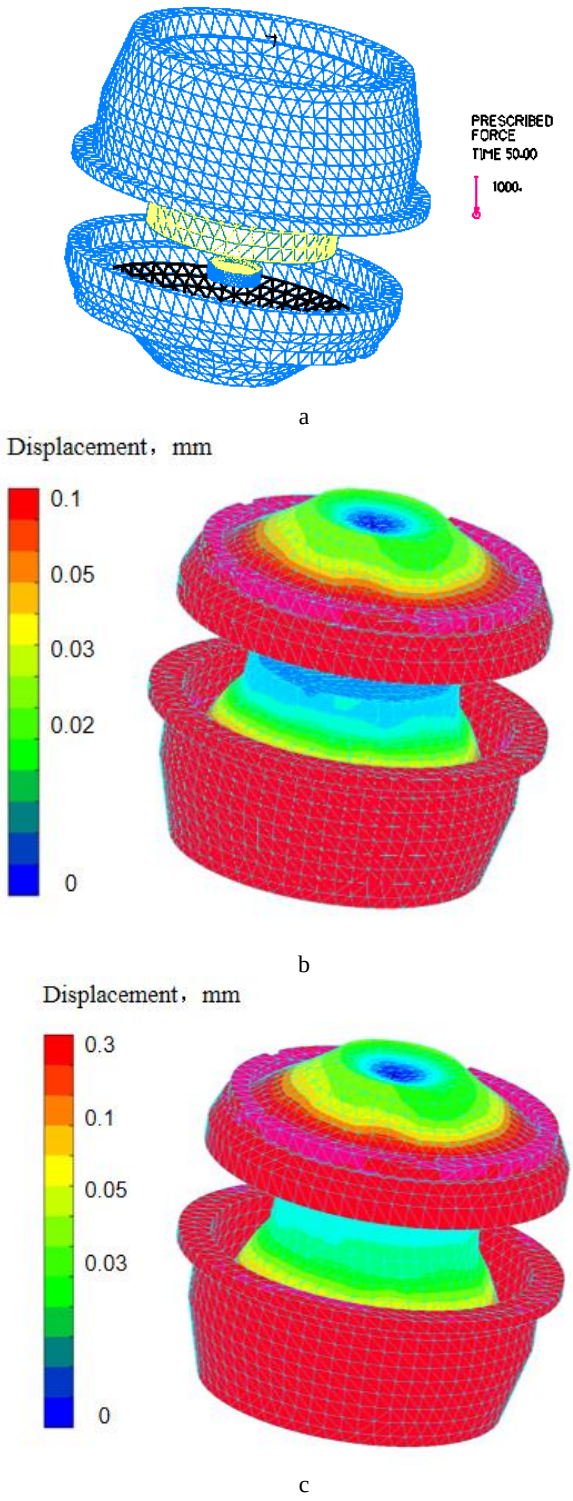


**Fig. 15.** Displacement nebulae of the solid part of MR mount: a – magnetorheological solid finite element model; b – minimum displacement cloud image; c-maximum displacement cloud image

To more intuitively grasp the deformation position of the preload, the cross-section displacement diagram of the magnetorheological mount is shown in Fig. 16. The finite element modeling method of Magnetorheological mount, especially the finite element modeling method considering multi-physical field coupling, is a further supplement to the research work in reference [10] and improves the accuracy of multi-physical field coupling analysis.

Because the magnetorheological mount has the effect of preload in the stiffness simulation, the displacement change of the rubber sole film is not obvious. It can be seen from the minimum displacement shown in Fig. 16 a that when the rubber main spring starts to carry out periodic force loading, its displacement is the minimum, and the displacement of the decoupling film has no obvious change.

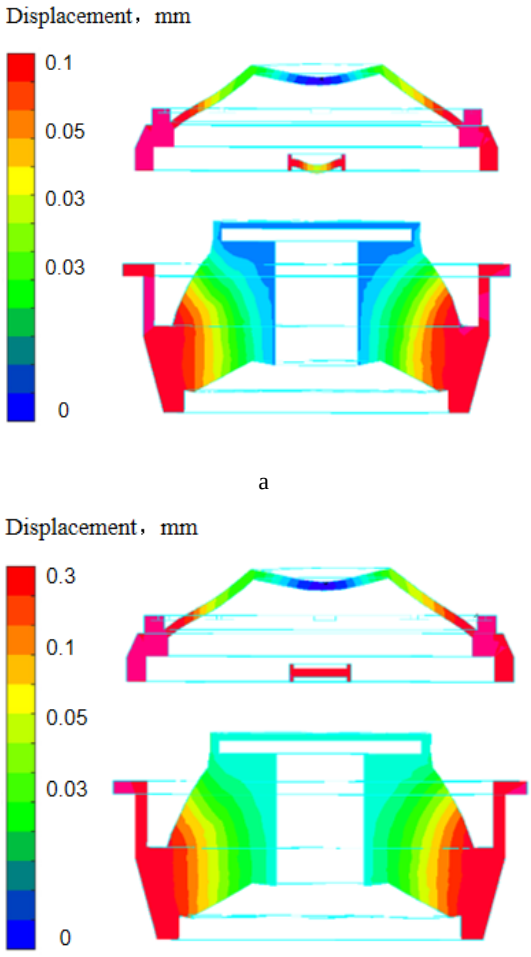


**Fig. 16.** Section of solid parts of MR mount: a – minimum displacement slice diagram; b – maximum displacement slice diagram

Fig. 16 b shows the cloud image when the MR mount displacement reaches the maximum. At this time, the decoupling film and the rubber main spring are subjected to the downward pressure of the liquid to reach the maximum stroke. This process accords with the theory of fluid-structure coupling. The modeling of the main spring, the loading of the preload force and the making of the planing diagram of the magnetorheological mount effectively solve the difficult problem of the dynamic modeling of the magnetorheological mount. The dynamic modeling of the magnetorheological mount in this paper effectively solves the difficult problem of finite element modeling proposed in reference [12, 13, 15]. The application of finite element modeling of magnetorheological mount is improved.

### 5.3.2. Fluid simulation analysis

The liquid in the magnetorheological mount is filled with the upper liquid chamber, the damping channel and the lower liquid chamber. In HyperMesh, the liquid is extracted from the contact wall of the main spring, damping channel and bottom film. The finite element solid model of magnetorheological liquid was built according to the finite element node fusion theory, and the fluid-structure coupling node fusion was carried out by ADINA.

The reciprocating movement of the rubber spring squeezes the fluid in the cavity, so that the stress of the magnetorheological fluid changes. Fig. 17 shows the stress variation diagram of the magnetorheological fluid in one stroke cycle of the rubber master spring.

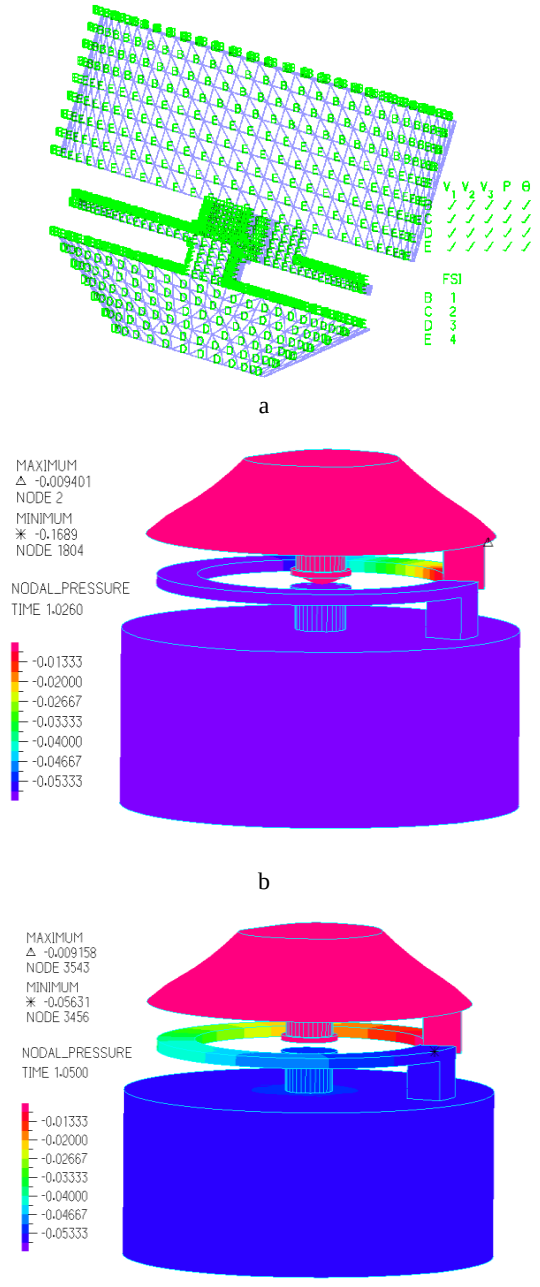


Fig. 17 continued on next page

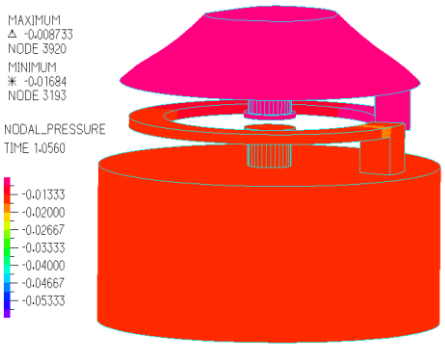


d

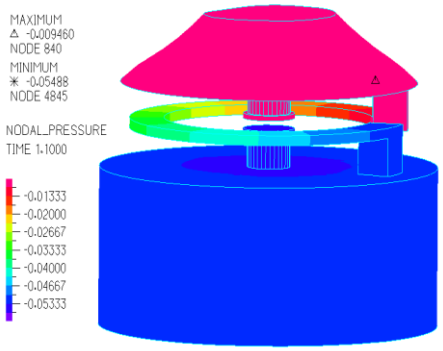


e

**Fig. 17.** Stress variation nephogram of MR Fluid in one cycle: a – construction of finite element model of magnetorheological liquid; b – nephogram of compressive stress at the beginning of the rubber main spring; c – nephogram of maximum displacement stress of rubber main spring; d – return stress nephogram of rubber main spring; e – stress nephogram of rubber master spring back to initial position

Under the action of preload, the strain simulation results of MR liquid in one cycle show that the maximum displacement of MR liquid ranges from -0.16 mm to -0.06 mm from the initial state to the maximum displacement state, and the displacement change is 0.1 mm. In a cycle period to restore the initial position, the overall displacement change is small. It can be seen from Fig. 17 that in one cycle of the movement of the rubber master spring, the stress on the MR fluid is always concentrated at the extruder end, and there is an obvious pressure gradient along the flow direction of the fluid.

The simulation results can provide a theoretical reference for magnetorheological mount liquid design. The finite element modeling theory of magnetorheological mount is constantly developing. Based on the fluid-solid coupling theory, this chapter discusses the finite element model construction and performance analysis optimization of magnetorheological liquid, and promotes the application of the new modeling method of Magnetorheological mount in reference [12]. Compared with reference [12], the pressure properties of magnetorheological mount liquids and the theory of liquid modeling were further studied.

## 5.4. Analysis of static and dynamic characteristics of MR mounting under magnetic field

### 5.4.1. Simulation analysis of static characteristics

The vertical static stiffness of the MR mount is analyzed, and the static load is gradually loaded from 0 to 1000 N. According to the simulation results of displacement and force, the static stiffness of the hydraulic mount can be calculated. Fig. 18 shows the static stiffness curve of the mount, which is 215 N/mm.

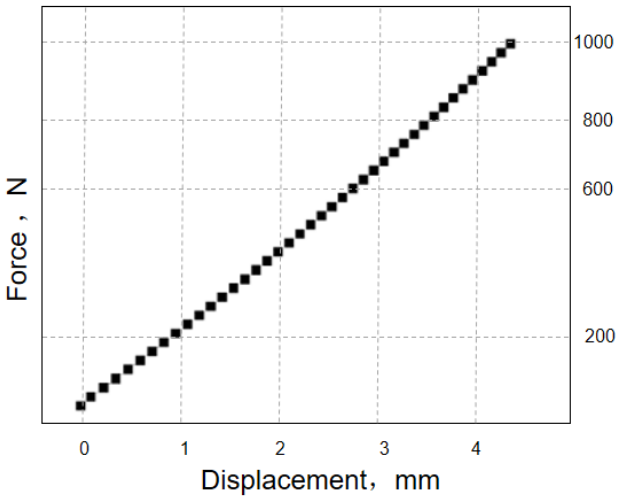


**Fig. 18.** Static stiffness curve

Fig. 19 shows asolid displacement and liquid stress diagram. The magnetorheological mount is designed to be mounted upside down with the engine under the rubber main spring. Its true motion state is that the engine exerts a downward force on the rubber main spring through the connecting rod. In this process, the space of the lower chamber becomes larger, and the liquid flows from the upper chamber to the lower chamber through the inertial channel under the action of pressure.

It can be seen from the magnetorheological solid displacement diagram that the maximum deformation of solid occurs at the rubber bottom film, and the maximum deformation reaches 5.6 mm. The maximum working deformation conforms to the design requirements of the MR mount [13]. It can be seen from the magnetorheological fluid diagram that the pressure distribution in the upper and lower chambers is uniform due to the slow liquid flow during the static stiffness simulation. In the inertial channel, the pressure of the magnetorheological liquid in the flow process drops in a uniform gradient and gradually decreases, which is consistent with the pressure distribution of liquid flow in the magnetorheological laminar flow theory [13, 15]. The maximum deformation of magnetorheological liquid is 0.06 mm, and the pressure distribution is uniform. This study can serve as a typical basis for subsequent modeling and optimization of MR fluids and provide a basis for the development of advanced simulation technology for MR mount, and is an effective supplement to the finite element modeling method of MR Described in literature [13].

### 5.4.2. Simulation analysis of dynamic characteristics

Dynamic stiffness is the main evaluation index of dynamic characteristics of magnetorheological mounting. In

the simulation analysis of dynamic characteristics, the preload is 1000 N and the amplitude is 0.5 mm.

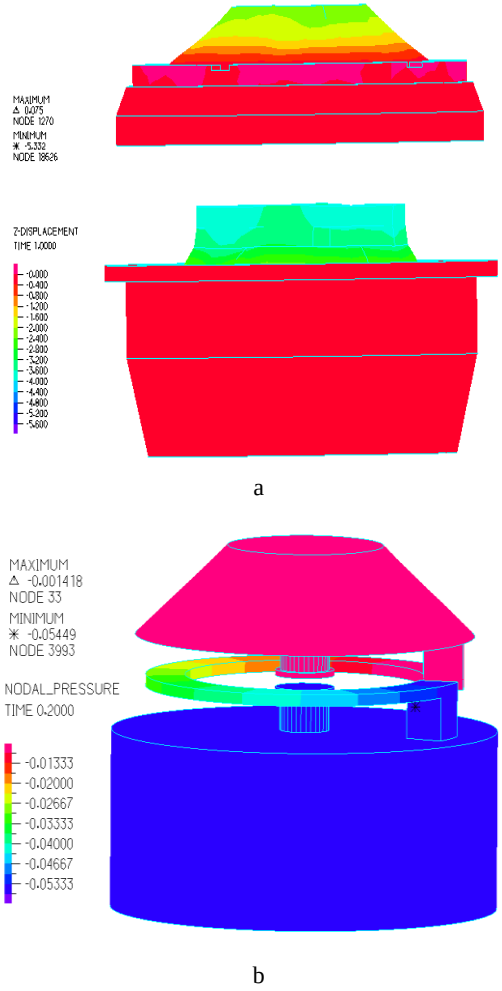


**Fig. 19.** Cloud image of static stiffness simulation: a – solid partial displacement cloud image; b – liquid part pressure cloud

After the simulation calculation is completed, the displacement and force data of the coupling point are derived in the ADINA post-processing module, and the hysteresis loop as shown in Fig. 20 can be obtained through data processing.

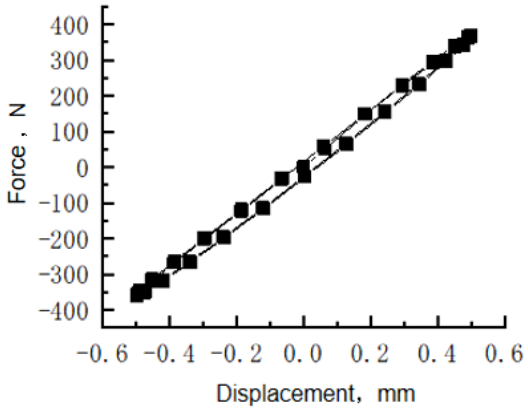


**Fig. 20.** 10Hz hysteresis curve

Similarly, the dynamic stiffness curve of the hydraulic mount can be plotted by simulating the excitation of other frequencies. The dynamic stiffness of the mount at each frequency is obtained, and the dynamic stiffness curve of the whole frequency range is finally obtained. The simulation curve of the variable stiffness of magnetic current under different current conditions is shown in Fig. 21.

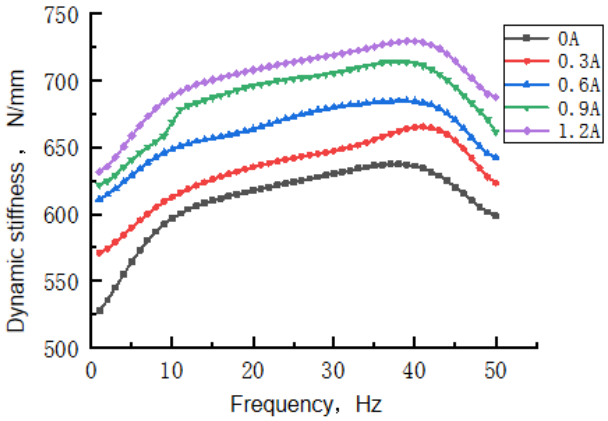


**Fig. 21.** Dynamic stiffness under different current

It can be seen from the figure that the viscosity of MR fluid increases with the increase of current. The viscous damping force and coulomb damping force increase with the increase of the flow rate in the damping channel. The stiffness of the MR mount increases with the increase of current (0 A – 1.2 A). When the current is 1.2 A, the maximum variable stiffness of the magnetic current is 720 N/mm. In MR mode, the mount stiffness can be increased by 1.2 times. The magnetorheological stiffness can be controlled by adjusting the current intensity to achieve variable stiffness characteristics. The dynamic stiffness electrified mode designed in this paper can increase 120 N/mm at most, which provides a reference for MR stiffness design and verifies the stiffness design trend under MR electrified mode [13, 15].

## 6. CONCLUSIONS

To accurately predict the structural properties of metal and rubber in magnetorheological fluids, design and optimize the nonlinear magnetization law and solid-liquid interaction between magnetorheological fluids and soft magnetic materials, and establish the mathematical and simulation models of electromagnetic coupling and fluid-structure coupling of magnetorheological fluids. The validity of the mathematical model is verified by magnetic rheological tests. On this basis, the magnetic field distribution in the magnetic circuit of magnetorheological metal and rubber structures is analyzed. According to the Bingham model, the variation rule of magnetorheological fluid viscosity was deduced. By introducing the magnetic field simulation results into the fluid model and the fluid-solid model respectively, the stress distribution of magnetorheological fluid in the damped channel under different magnetic fields is calculated. The dynamic properties of magnetorheological structures under different current currents are studied. In this paper, the multi-physical field fluid-solid-magnetic coupling analysis and finite element modeling of magnetorheological liquid have been extended, which has promoted the development of the subject. The stress analysis of magnetorheological fluid verifies the uniformity of magnetorheological fluid flow, and provides ideas for designing magnetorheological fluid.

The viscosity characteristics and design rules of magnetorheological liquids are discussed, and the development idea of the subject is expanded. Through the above research, the main research results are as follows:

1. The magnetorheological stiffness can be controlled by current adjustment with a magnetorheological mount. The variable stiffness value of magnetic current increases with the increase of input current. The controllable damping force increases with the increase of current. When the input current increases from 0.9 A to 1.2 A, the stiffness does not change significantly. When the magnetic saturation operating point is reached at 1.2 A, the dynamic stiffness value no longer increases. When the maximum input current is 1.2 A, the dynamic stiffness reaches a peak of 827 N/mm.
2. The stress distribution of magnetorheological liquid under preload is uniform. The maximum displacement change of the magnetorheological liquid from the initial state to the main spring movement period is 0.1 mm. During the movement period of the main spring, the stress of MR fluid is concentrated at the extrusion end of the structure, and there is a pressure gradient along the flow direction. The stress distribution of magnetorheological fluid and the method of liquid modeling have expanded the finite element modeling method of magnetorheological fluid and promoted the development of the discipline.
3. In the current excited magnetorheological mount, the viscosity of the magnetorheological fluid increases with the increase of the current, and the viscous damping force and coulomb damping force provided by the flow in the damped channel also increases. The magnetorheological viscous stiffness of the current limit value can reach 725 N/mm. The finite element modeling method of magnetorheological liquids and the viscous stiffness verification provide the basis for the design of magnetorheological liquids and promote the development of magnetorheological design.
4. The magnetorheological stiffness is controlled by adjusting the current intensity to realize the variable stiffness characteristic. The designed magnetorheological model can increase the maximum stiffness by 120 N/mm, which can provide a reference for the variable stiffness design of magnetorheological structures.
5. The research results provide a theoretical basis for the design of metal and rubber structures of MR mount, and provide a theoretical basis for the design of MR liquid modeling and simulation, the pressure distribution stress of MR liquid and the distribution law of MR magnetic intensity. It provides the basis for the design of magnetorheological systems and promotes the development of magnetorheology.

## *Acknowledgments*

The research was financially supported by the Hubei Superior and Distinctive Discipline Group of "New Energy Vehicle and Smart Transportation".

**REFERENCES**

1. **Morato, M.M., Pham, T.P., Sename, O., Dugard, L.** Development of A Simple ER Damper Model for Fault-tolerant Control Design *Journal of the Brazilian Society of Mechanical Sciences and Engineering* 42 2020: pp. 1 – 22. https://doi.org/10.1007/s40430-020-02585-y
2. **Pham, T.P., Sename, O., Dugard, L., Vu, V.T.** LPV Force Observer Design and Experimental Validation from A Dynamical Semi-Active ER Damper Model *IFAC-Papers on Line* 52 (17*)* 2010: pp. 60 – 65. https://doi.org/10.1016/j.ifacol.2019.11.027
3. **Nguyen, Q.H., Choi, S.B., Lee, Y.S., Han, M.S.** Optimal Design of High Damping Force Engine Mount Featuring MRF Valve Structure with Both Annular and Radial Flow Paths *Smart Materials and Structures* 22 2013: pp. 1 – 10. https://doi.org/10.1088/0964-1726/22/11/115024
4. **Hu, Y.** Research on Magnetorheological Mount of Automobile Engine. Chongqing University Press, Chongqing, 2008: pp. 1 – 124.
5. **Li, Y.** Method and Experimental Study of Engine Vibration Isolation Based on Magnetorheological Fluid mount Chongqing University Press, Chongqing, 2009: pp. 1 – 103.
6. **Ciocanel, C., Elahinia, M.** Design and Modeling of A Mixed Mode Magnetorheological (MRF) Fluid Mount *Proceedings of SPIE – The International Society for Optical Engineering* 6928 2008: pp. 1 – 10. https://doi.org/10.1117/12.775993
7. **Bodie, M.O., Long, M.W.** MRF-Fluid Hydraulic Mount United States Standard US7510061 B2, 2009.
8. **Tharehalli, M.G., Kumar, H., Mahalingam, A.** Performance Analysis of a Semi-active Suspension System Using Coupled CFD-FEA Based non-Parametric Modeling of Low Capacity Shear Mode Monotube MR damper *Proceedings of The Institution of Mechanical Engineers Part D Journal of Automobile Engineering* 2018: pp. 1 – 10. https://doi.org/10.1177/0954407018765899
9. **Yu, Z.** Multi-field Coupling Analysis and Control System of MR Semi-active Shock Absorber. Jilin University Press, Changchun, 2014: pp. 1 – 156.
10. **Song, L.** Study on Mechanical Properties of Magnetorheological Dampers in Multiple Physical Fields. Harbin Engineering University Press, Harbin, 2008: pp. 1 – 143.
11. **Farzad, R., Bahman, F.A., Hedayat, V., Siamak, T.** An Inverse TSK Model of MRF Damper for Vibration Control of Nonlinear Structures Using an Improved Grasshopper Optimization Algorithm *Structures* 26 2020: pp. 406 – 416. https://doi.org/10.1016/j.istruc.2020.04.026
12. **Jolly, M. R., Carlson, J.D., Muoz, B.C.** A Model of the Behaviour of Magnetorheological Materials *Smart Materials and Structures* 5 1996: pp. 607 – 614. https://doi.org/10.1088/0964-1726/5/5/009
13. **Park, J.H., Park, O.O.** Electrorheology and Magnetorheology *Korea-Australia Rheology Journal* 13 2001: pp. 13 – 17. https://doi.org/10.1117/12.775993/009
14. **Carlson, J.D., Weiss, K.D.** A Growing Attraction to Magnetic Fluids *Machine Design 66* 1994: pp. 61 – 64. https://doi.org/10.1016/0273-1177(84)90161-3
15. **Poznic, A., Miloradovic, D., Juhas, A.** A New Magnetorheological Brake`s Combined Materials Design Approach *Journal of Mechanical Science and Technology* 31 2017: pp. 1 – 7. https://doi.org/10.1007/s12206-017-0210-5